International Journal of Solids and Structures 49 (2012) 3616–3625

Contents lists available at SciVerse ScienceDirect

International Journal of Solids and Structures

journal homepage: www.elsevier.com/locate/ijsolstr

# Path independent forming limits in strain and stress spaces

Thomas B. Stoughton [a], Jeong Whan Yoon [b,*]

[a] Manufacturing Systems Research Lab, MC 480-106-359, General Motors R& D Center, Warren, MI 48090-9055, United States
[b] Faculty of Engineering & Industrial Sciences, Swinburne University of Technology, Hawthorn, VIC 3122, Australia

ARTICLE INFO

*Article history:*
Available online 17 August 2012

*Keywords:*
Strain FLC
Stress-based FLC
Polar EPS diagram
Necking limit

ABSTRACT

Many practitioners of the metal forming community remain faithful to the idea that strain metrics are useful for formability assessment, while many others who are aware of the limitations of strain metrics are nevertheless reluctant to use stress metrics because of concerns about their practicality. In this work, we review the stress-based forming limit approach and discuss the major history-dependent parameters explicitly accounting for non-linear deformation in the stress space. Then, the parameters are consistently considered in the strain spaces and a new type of forming limit diagram based on a polar representation of the EPS (Effective Plastic Strain) is proposed that has advantages of both stress and strain metrics. The Polar Effective Plastic Strain (PEPS) appears to be an effective solution to the problem of non-linear effects, with advantages of the familiar strain-based diagram for linear loading, and without the strain-hardening limitations of the stress diagram, or non-intuitive aspects of the alternate Cartesian diagrams based on effective plastic strain.



## 1. Introduction

It continues to be argued explicitly or implicitly that strain paths in most metal forming applications, and particularly in the first draw die, are sufficiently linear that the initial strain FLC for the as-received condition can be used without serious risk of error in making formability assessments. In fact, with the exception of axisymmetric and uniform sectioned parts, studies of industrial applications show that most of the strains in automotive applications that reach levels of plastic strain that would be considered at risk for failure, also include a substantial nonlinear component in the strain history. Nonlinear strain paths occur in every region of late contact with 3D tooling surfaces, as well as in areas in which the metal flows from one region of the tool geometry to another. While nature tends to take the shortest and therefore linear path, the complex 3D geometries into which we attempt to form metal do not allow metal to be stretched to high strains by linear paths, except in very rare circumstances.

Perhaps the most serious limitation of the initial strain FLC is shown in Fig. 1 presented by Graf and Hosford (1993) experimentally. However, it may not be immediately obvious how serious the problem is because it is often argued that the complex pattern of strain FLCs shown here do not apply when strain paths are linear or "nearly linear". But that argument is seriously misinterpreting what the data in Fig. 1 means. All of the FLC's in this figure are actually characterization of the evolving strain FLC for linear paths. To understand this meaning, consider, for example, the following four FLC's in Fig. 2(a) shown for uniaxial tension along the transverse direction directly taken from Fig. 1: (1) the black FLC with FLDo at a longitudinal strain of about 0.19, (2) the tan-colored FLC with a cusp close to the horizontal axis at a transverse strain of 0.07, (3) the blue FLC with a cusp close to a transverse strain of 0.13, and (4) the red FLC with a cusp at a transverse strain of about 0.17. The set of all four of these curves define the evolution of the "single" FLC for a linear strain path corresponding to uniaxial strain along the transverse direction. Fig. 2(b) shows the evolution of the stain FLC for a linear strain path corresponding to uniaxial strain along the rolling direction for the four curves taken from Fig. 1.

What this data means is the strain FLC for linear strain path is not static, but is an intrinsically dynamic limit. This is not semantic difference. It has serious consequences on the use and utility of the initial strain FLC. It means that the initial strain FLC for the as-received condition gives no clue about the margin of safety of a given forming process, regardless of whether the path is linear or non-linear. Once the implications of this data are understood, it cannot be rationally argued that the initial strain FLC can be used in conditions where the strain path is "almost" linear. The only point on the original FLC in the as-received condition that continues to apply for a linear strain path, is the endpoint of the linear strain path. The shape of the forming limit in all other directions from any point on the linear path is dramatically different from the shape of the original FLC. In view of that, few measures are more limited in application than the initial strain-FLC for materials in the as-received condition.

* Corresponding author. Tel.: +61 3 9214 5573.
*E-mail address:* jyoon@swin.edu.au (J.W. Yoon).

0020-7683/$ - see front matter © 2012 Elsevier Ltd. All rights reserved.
http://dx.doi.org/10.1016/j.ijsolstr.2012.08.004

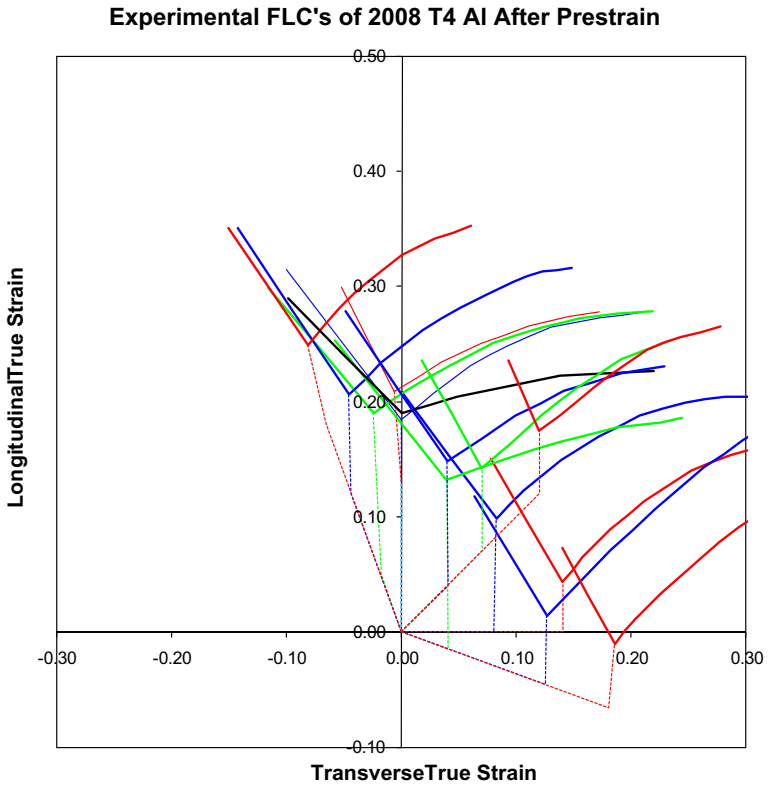


**Fig. 1.** Experimental FLC's of 2008 T4 AA reported by Graf and Hosford (1993) for the as-received and for 12 prestrain conditions.

Ishigaki (1977) at Toyota Motors Company first applied the concept of the dynamic strain path for improving the formability. As can be seen in Fig. 3, Toyota engineers achieved a remarkable improvement of the formability, reaching thinning strains of up to 60% with a net minor strain near to zero in a multi-stage forming process of a quarter panel, although the FLDo for the zero-prestrained condition of the metal used is only 37 % by taking advantage of the dynamic nature of the strain FLC. In the figure, the initial forming limit curve is denoted by the gray line. Toyota engineers recognized that at the end of stage 4, the gray curve is not valid as the formability limit. Coincidentally, the strain condition at the end of stage 4 in the location that would eventually tear, highlighted as the green point in Fig. 3 along the original path, happens to be very close to unixial tension conditions for this metal and also happens to be reached by an almost linear strain path. These two facts motivated the Toyota engineers to prestrain large sheets in uniaxial tension to 37% strain, and then experimentally determine the evolved shape of the forming limit curve for uniaxial tension to this level of strain. This experimentally determined FLC is shown as the red line in Fig. 3, and was then used by Toyota engineers as an estimate of the residual formability of the metal at the end of Stage 4 in the critical location. Based on the red curve, the deformation process was modified to drive the strain to follow a new biaxial path (rather than the original biaxial path that led to a failure) during stages 5 and 6 to dramatically improve the formbaility.

As can be seen in Fig. 3, the characterization of forming limits is a significant challenge in complex processes since the conventional strain-based FLC is sensitive to strain path. Practically, it is very difficult to trace the dynamic forming limit curves for each element in simulation. The most promising solution for dealing with strain-path effects in the FLC is to use a stress-based curve, as independently proposed by Arrieux et al. (1982), Stoughton (2000), Stoughton and Yoon (2005), Stoughton and Yoon (2011). These authors have shown that the stress-based FLC is not affected by strain path, and should be applicable without modification to analysis of all forming problems.

One of the concerns about the stress FLC is attributed to the reduction of the slope of the true stress-strain relation. Due to this effect, larger changes in strain occur at stress levels close to the necking limit compared to at stress levels further below the limit stress. This makes it difficult to visually see or quantify the margin of safety without a magnifying glass or overlay of the contours of equivalent strain in the stress FLC. To remedy this difficulty, we will propose the effective plastic strain as one of the metrics to assess formability following a modification of the idea proposed by Zeng et al. (2008). Although the effective plastic strain is described as a type of strain, it is not directly linked to the principal or tensor components of the strain tensor. It is however, uniquely linked to the stress tensor through the yield function and stress-strain relation, and therefore falls under the category of a stress metric. A path-independent Polar Effective Plastic Strain (PEPS) diagram is newly suggested in this work. It will be proved that the Polar EPS Diagram has a one-to-one mathematical correspondence to the stress-Based FLC. And it will also be demonstrated from experimental data that the forming limit curve in the PEPS diagram is insensitive to changes in strain path. The PEPS diagram can be a powerful tool to design nonlinear paths to maximize the formability.

## 2. Review of Stress-Based FLC

A representation of the forming limit behavior for proportional loading in strain space, i.e., the locus of principal strains, is specified as follows.

$$strain - FLC = \begin{bmatrix} e_1^{FLC} \\ e_2^{FLC} \end{bmatrix} = e_1^{FLC} \begin{bmatrix} 1 \\ \beta \end{bmatrix} \tag{1}$$

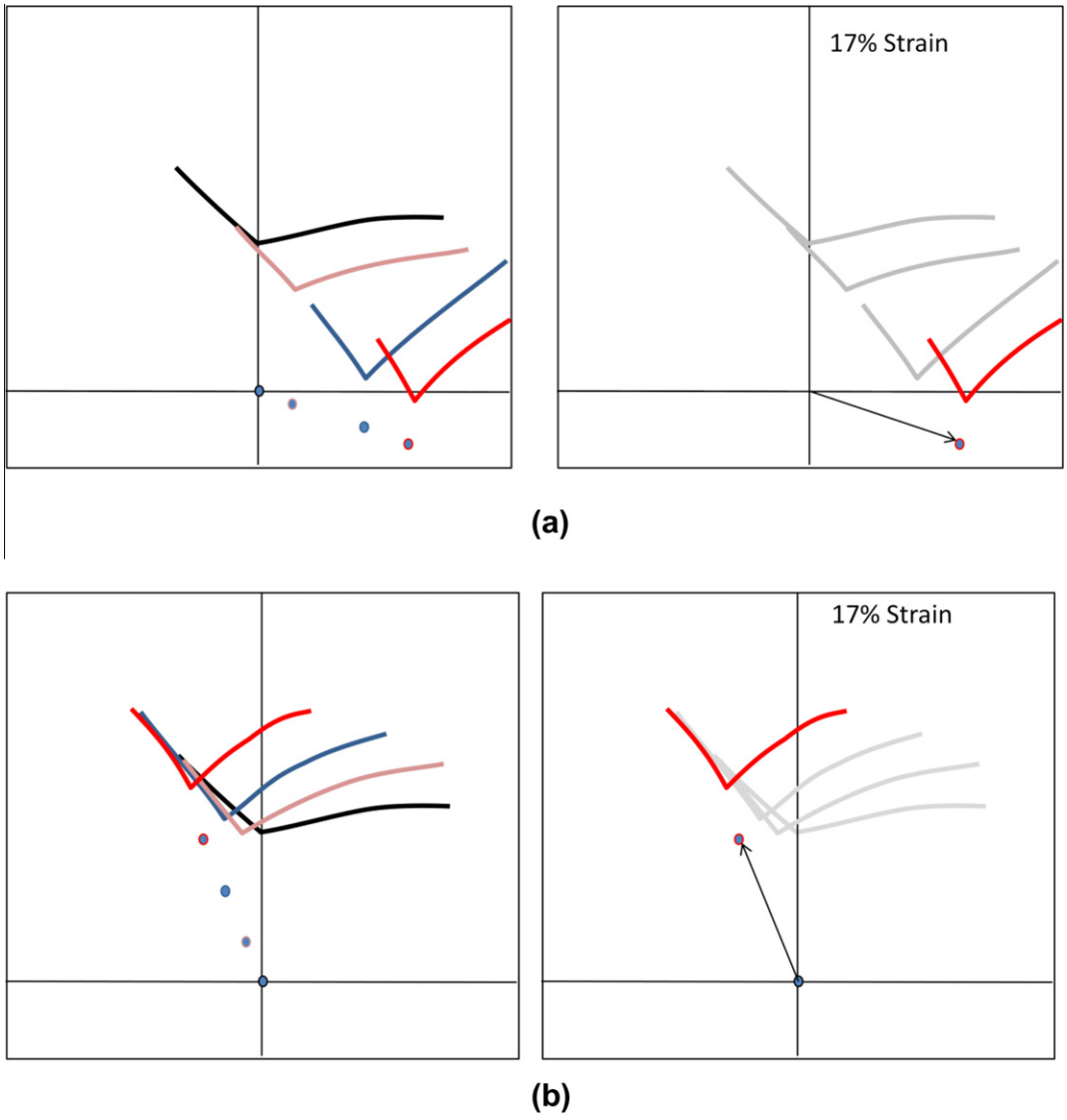


**Fig. 2.** Movement of experimental strain FLC under uniaxial tensions taken from Fig. 1 (a) along the transverse direction (b) along the rolling direction.

where $\beta(=\dot{e}_2^{FLC}/\dot{e}_1^{FLC})$ , is a parameter in the range $\beta = [-1, +1]$ that defines the ratio of the plastic principal in-plane strain rates. For a point on the strain FLC for a linear strain path, $\beta$ is a constant given by the ratio of the plastic strains at the point. A serious limitation of the strain-based FLC is that it applies only to cases of proportional loading, and will lead to a false assessment when the strain-path is highly non-linear. A solution to this issue is to use the stress-based FLC, which has been shown to be independent of loading history. This section reviews how to derive the stress-based forming limit criterion from the strain-based FLC based on Hill's (1948) model for a metal with normal anisotropy. The derived equations will be used to explain the history dependent variables accounting for nonlinearity in the Section 4.

The minor principal stress, $\sigma_2^{FLC}$, is proportional to the major stress by a parameter $\alpha = [-1, +1]$, i.e.,

$$\sigma_2^{FLC} = \alpha\sigma_1^{FLC}. \tag{2}$$

Note that with the specified range for the $\alpha$ parameter, the magnitude of the minor principal stress is always less than or equal to the major stress. The major principal stress can be used as a normalizing factor in the following derivation without concern about singularities in the calculations.

Hill's (1948) yield function for normal anisotropy under plane stress is defined in terms of the principal stress as (Hill, 1948)

$$\bar{\sigma}(\sigma_1^{FLC}, \sigma_2^{FLC}) = \sqrt{(\sigma_1^{FLC})^2 + (\sigma_2^{FLC})^2 - \frac{2\bar{r}}{1+\bar{r}}\sigma_1^{FLC}\sigma_2^{FLC}} \tag{3}$$

where $\bar{r}$ is the averaged r-value. The ratio of the major and minor principal stresses defines the parameter $\alpha$ as implied by Eq. (2). Then Eq. (3) can be written as

$$\bar{\sigma} = \sigma_1^{FLC}\sqrt{1+\alpha^2 - \frac{2\bar{r}}{1+\bar{r}}\alpha} \tag{4}$$

or

$$\frac{\bar{\sigma}}{\sigma_1^{FLC}} = \sqrt{1+\alpha^2 - \frac{2\bar{r}}{1+\bar{r}}\alpha} = \bar{\sigma}_\alpha(1,\alpha). \tag{5}$$

By using the associated flow rule with Eq. (4), the major and minor plastic strains under linear strain paths can be defined as

$$\dot{e}_1^{FLC} = \dot{\bar{\varepsilon}}_p^{FLC}\frac{\partial\bar{\sigma}}{\partial\sigma_1^{FLC}} = \dot{\bar{\varepsilon}}_p^{FLC}\left(\frac{\sigma_1^{FLC}}{\bar{\sigma}}\right)\left(1 - \frac{\bar{r}}{1+\bar{r}}\alpha\right) \tag{6 - 1}$$

$$\dot{e}_2^{FLC} = \dot{\bar{\varepsilon}}_p^{FLC}\frac{\partial\bar{\sigma}}{\partial\sigma_2^{FLC}} = \dot{\bar{\varepsilon}}_p^{FLC}\left(\frac{\sigma_1^{FLC}}{\bar{\sigma}}\right)\left(\alpha - \frac{\bar{r}}{1+\bar{r}}\right) \tag{6-2}$$

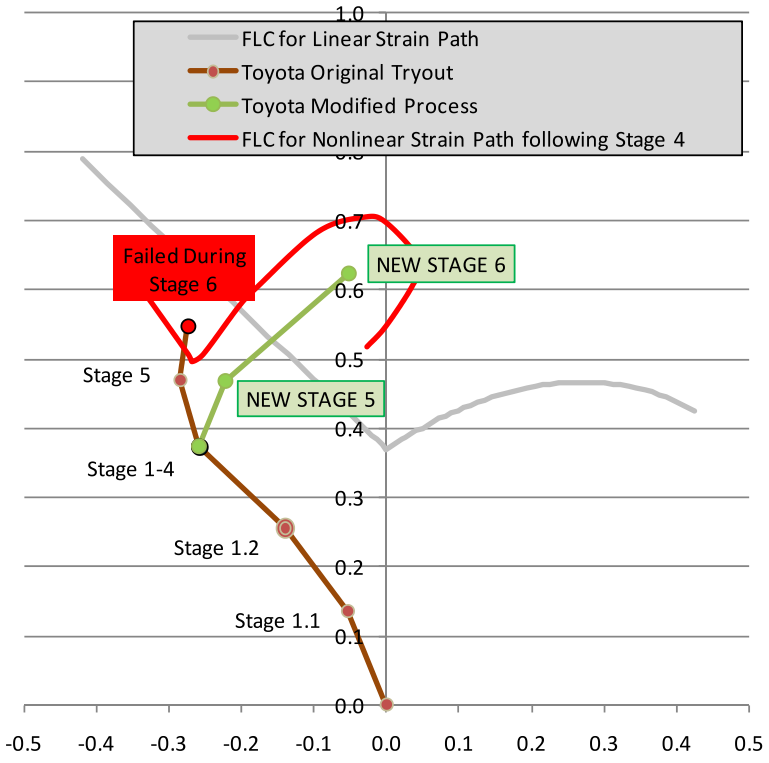


**Fig. 3.** Nonlinear strain path concept developed by Toyota and applied to tryout of a quarter panel stamped from a deep draw quality steel. Forming limit curves are experimental (Ishigaki, 1977).

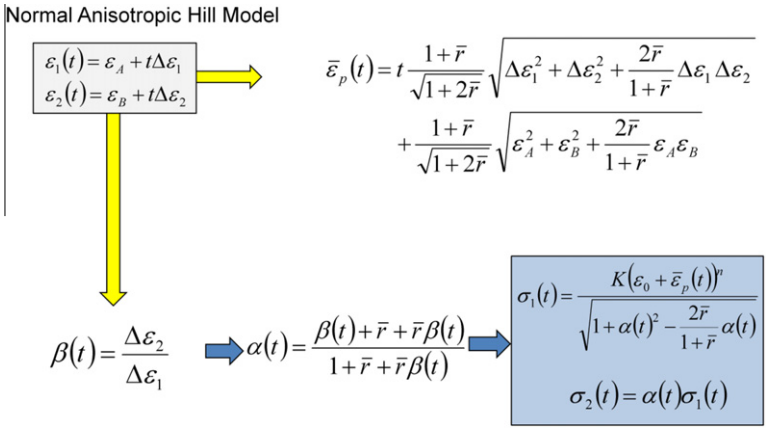


**Fig. 4.** Mapping procedure from plastic strain FLC to Stress FLC for a bi-linear strain path from $(\varepsilon_A,\varepsilon_B)$ with final increment $(\Delta\varepsilon_A,\Delta\varepsilon_B)$.

Then, the principal strain ratio, $\beta$ is defined as a function of the principal stress ratio $\alpha$ as

$$\beta=\frac{\dot{e}_2^{FLC}}{\dot{e}_1^{FLC}}=\frac{\frac{\partial\bar{\sigma}}{\partial\sigma_1^{FLC}}}{\frac{\partial\bar{\sigma}}{\partial\sigma_2^{FLC}}}=\frac{\alpha+\bar{r}\alpha-\bar{r}}{1-\bar{r}\alpha+\bar{r}}. \tag{7-1}$$

Alternatively,

$$\alpha=\frac{\beta+\bar{r}+\bar{r}\beta}{1+\bar{r}+\bar{r}\beta} \tag{7-2}$$

On the other hand, the effective plastic strain at necking can be also defined by adding Eqs. (6-1) and (6-2) and rearranging terms as

$$\dot{\bar{\varepsilon}}_p^{FLC}=\frac{\dot{e}_1^{FLC}+\dot{e}_2^{FLC}}{\frac{\partial\bar{\sigma}}{\partial\sigma_1^{FLC}}+\frac{\partial\bar{\sigma}}{\partial\sigma_2^{FLC}}}=\frac{(1+\beta)\dot{e}_1^{FLC}}{\sqrt{1+\alpha^2-\frac{2\bar{r}}{1+\bar{r}}\alpha}}\left(\frac{1+\bar{r}}{1+\alpha}\right). \tag{8}$$

By inserting Eq. (7-2) into Eq. (8), the strain-rate potential for Hill's (1948) normal anisotropic yield function can be derived as

$$\dot{\bar{\varepsilon}}_p^{FLC}=\frac{1+\bar{r}}{\sqrt{1+2\bar{r}}}\sqrt{\left(\dot{e}_1^{FLC}\right)^2+\left(\dot{e}_2^{FLC}\right)^2+\frac{2\bar{r}}{1+\bar{r}}\dot{e}_1^{FLC}\dot{e}_2^{FLC}}. \tag{9-1}$$

or

$$\bar{\varepsilon}_p^{FLC}=\int_0^t\dot{\bar{\varepsilon}}_p^{FLC}dt \tag{9-2}$$

Using a hardening law and Eq. (5),

$$\bar{\sigma}=\sigma_1^{FLC}\bar{\sigma}_\alpha(1,\alpha)=h\left(\bar{\varepsilon}_p^{FLC}\right) \tag{10-1}$$

where

$$h\left(\bar{\varepsilon}_p^{FLC}\right)=K\left(\varepsilon_o+\bar{\varepsilon}_p^{FLC}\right)^n \text{ or } h\left(\bar{\varepsilon}_p^{FLC}\right)=A-B\exp\left(-C\bar{\varepsilon}_p^{FLC}\right) \tag{10-2}$$

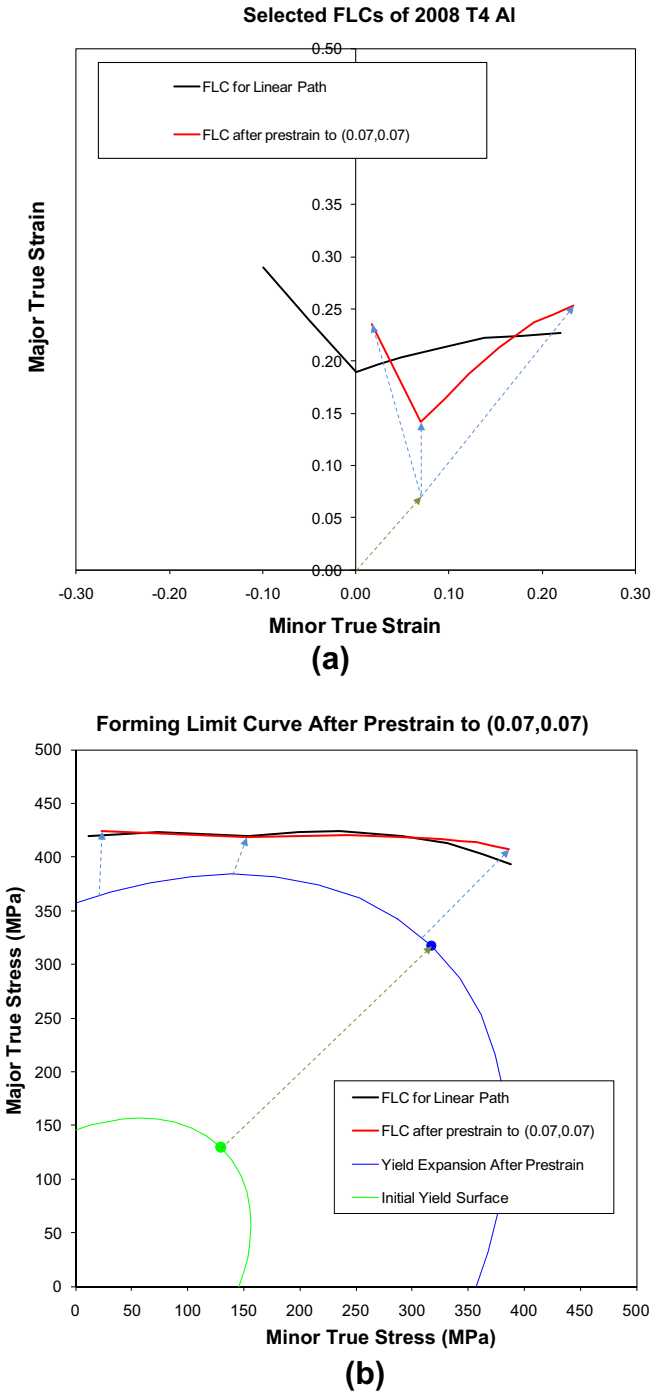


**Fig. 5.** Experimental forming limit curves for linear strain paths and for a bilinear strain path after 0.07 strain in equal biaxial tension in (a) strain and (b) stress spaces. The green dashed lines with arrows in both figures show the corresponding strain and and calculated stress increments due to prestrain and three blue dashed lines show selected strain and corresponding calculated stress increments to the final point on the strain FLC. Note that the overlay of the two experimental stress FLCs is proof that stress-based FLCs are independent of the loading history.

we can finally calculate the major principal stress; i.e.,

$$\sigma_1^{FLC} = \frac{h\left(\bar{\varepsilon}_p^{FLC}\right)}{\bar{\sigma}_\alpha(1,\alpha)} = \frac{h\left(\bar{\varepsilon}_p^{FLC}\right)}{\sqrt{1+\alpha^2-\frac{2\bar{r}}{1+\bar{r}}\alpha}} \tag{10-3}$$

and the minor principal stress using Eq. (2).

The equations for calculating the effective plastic strain and principal stresses for an arbitrary bilinear plastic strain path is shown in Fig. 4 for a special case of Hill's (1948) normal anisotropy. Fig. 4 generalizes the mapping procedure from the principal plastic strain-space to the principal stress space for arbitrary bilinear plastic strain increments to an intermediate strain state, $(e_1,e_2) = (e_A,-e_B)$, ending at a final plastic strain state, $(e_A+\Delta e_1, e_B+\Delta e_2)$. An example of this transformation for two of the FLCs shown for 2008 T4 taken from Fig. 1 is shown in Fig. 5. In the figure, the red curve is the FLC for the condition of zero-prestrain. The FLC for a bilinear path with an equal-biaxial plastic pre-strain $(e_1,e_2) = (0.07,0.07)$ is shown in purple. There is no significant difference in the calculated stress FLCs for linear and nonlinear strain paths seen in Fig. 5. Since these FLCs are determined from experiment, the analysis leads to the conclusion that stress-based forming limits are insensitive to the deformation history, and depend only on the stress state. This surprising result of a path independent stress-based forming limit is theoretically validated by review of bifurcation analyses that were originally used to explain the strain FLC, as explained in Stoughton and Zhu (2004). It is shown in this reference that the bifurcation models lead to an instability condition that can be conveniently expressed explicitly in terms of the current state of the true stress, without explicit dependence on any history variables. This result occurs prior to imposing any assumption on the strain path that may have been involved to reach the critical stress condition at which the instability will occur, which of course is necessary to derive a strain forming limit criterion for a given strain path.

Fig. 6 generalizes the mapping procedure from the principal plastic strain-space to the principal stress space for arbitrary plastic strain histories, $(e_1,e_2) = (e_1(t),e_2(t))$. The general equations to derive the effective plastic strain and principal stresses for a non-quadratic yield function or other yield functions with planar anisotropy are described in Stoughton and Yoon (2005).

## 3. Use of Stress-Based Necking Limit from FEM Results

Arrieux et al. (1982) were among the first to publish evidence that the dynamic nature of the strain FLC for steel arises from a single path-independent stress limit in combination with the non-unique relationship between the loading stress and net plastic strain tensor components. They were also among the first to propose using the stress FLC in formability analysis. This discovery has been shown by others to apply to all metals, including the AA 2008 T4 used in Graf and Hosford (1993) work shown in Fig. 1, as reported in Stoughton (2000), from which the data shown in Fig. 5 is taken. The final stress conditions on each of these strain FLCs appears to be consistent with a single stress FLC, within experimental uncertainty. Based on these and similar experimental studies, it is concluded that the stress condition appears to be the casual factor in the initiation of necking. More importantly, the result supports a simple practical solution to the ambiguity of strain forming limits in manufacturing; As long as the stress condition is maintained below this single stress FLC, the forming process will be safe from necking. So the stress FLC satisfies the need of industry for a simple diagram to clearly separate safe and non-safe forming conditions, much as the strain FLC is currently misused today. Although this FLC is apparently path-independent, the stresses calculated in the finite element (FE) analysis are process dependent variables. Therefore, it is necessary to monitor the stress state at each step of the computation and determine if the current state is below or above the stress-based FLC. For this purpose, it is convenient to use a single parameter to monitor the formability margin as described in

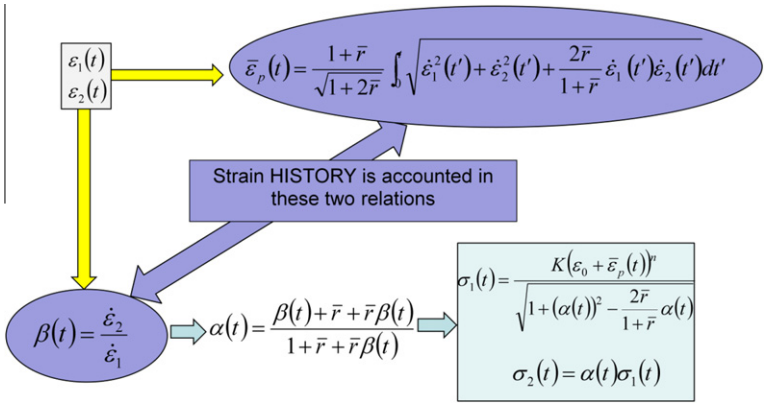


**Fig. 6.** Equations for normal anisotropic model and variables which account for strain history.

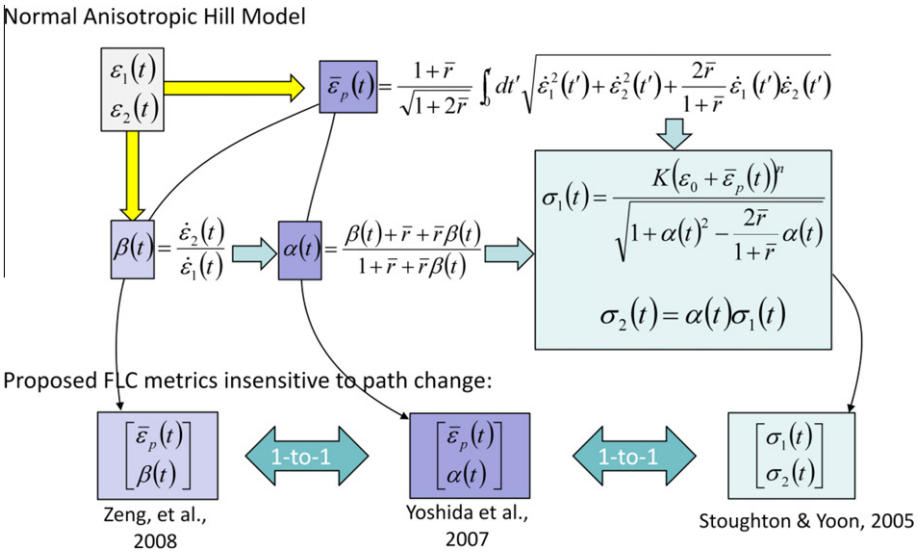


**Fig. 7.** One-to-one correspondence among path-independent formability models.

Stoughton and Yoon (2005). The formability parameter $\gamma_C$, defined in terms of critical stress ratios, is defined as follows,

$$\gamma_C = \begin{cases} \frac{\bar{\sigma}_Y(\sigma_i)}{h\left(\bar{\varepsilon}_p^{FLC}\right)} & \sigma_1+\sigma_2 > 0 \\ 0 & \sigma_1+\sigma_2 \leqslant 0 \end{cases} \tag{11}$$

The steps necessary to calculate $\gamma_C$ from the principal stresses $(\sigma_1,\sigma_2)$ are are follows

(1) The stress ratio $\alpha$ and strain-rate ratio $\beta$ are calculated using Eqs. (2) and (7-1) sequentially.
(2) The value of the major strain on the strain FLC in the direction $\theta = \tan^{-1}(\beta)$ is obtained from the representation of the strain FLC curve,
(3) The effective plastic strain on the FLC at this point is calculated using Eq. (9).
(4) The yield stress at this point on the FLC is calculated using the appropriate hardening law, such as one of the two given in Eq. (10-2).
(5) The ratio, $\gamma_C$, of the current value of the yield function and the current value of the yield stress at the necking limit in the direction of the current stress, is calculated.

The parameter $\gamma_C$ serves as a single stress scaling parameter that represents the degree of formability according to the criteria $\gamma_C < 1$ (safe) or $\gamma_C > 1$ (neck).

## 4. The Polar Effective Plastic Strain Diagram

To understand the history dependent variables for non-linear deformation, it is helpful to more carefully review the mapping procedure from plastic strain space to stress space as illustrated in Fig. 6. It is useful to point out that that the accounting of nonlinear paths comes into play at only two places. The first is in the definition of $\beta$, which for non-linear strain paths is defined in terms of the ratio of the current strain *rates*. Nonlinear paths also play a role in the definition of the effective plastic strain $\bar{\varepsilon}_p$, which is defined by the time integral of a function of the strain *rates*. This integration is complicated by the fact that $\beta$ is also changing in time. No other relation depends explicitly on deformation history. Since the stress tensor components are then defined explicitly in terms of the effective plastic strain and $\alpha$, or indirectly in terms of the effective plastic strain and $\beta$, the forming limit for linear and non-linear deformations can also be characterized as a simple limit on the accumulated effective plastic strain, $\bar{\varepsilon}_p$, as a function of $\beta$, or as a function of $\alpha$.

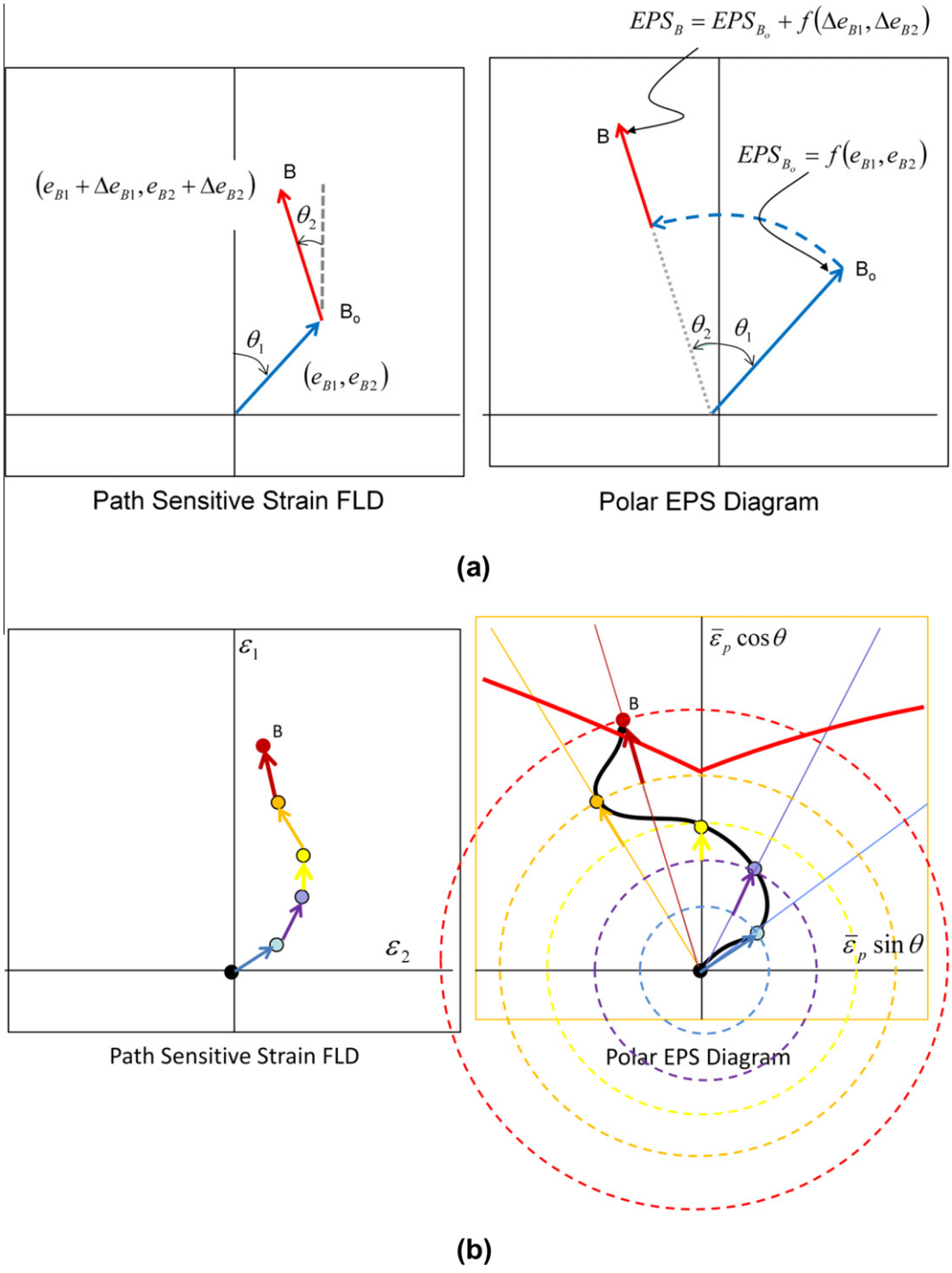


**Fig. 8.** Graphical illustrations of Polar EPS Diagram (a) bi-linear path (b) arbitrary path.

One of the concerns about the stress FLC is the reduction of the slope of the true stress-strain relation. Due to this effect, larger changes in strain occur at stress levels close to the necking limit compared to at stress levels further below the limit stress. This makes it difficult to visually see or quantify the margin of safety in the stress diagram without a magnifying glass or overlay of the contours of equivalent strain in the stress FLC. To remedy this difficulty, we will consider using the effective plastic strain as one of the metrics to assess formability. Although effective plastic strain is described as a type of strain, it is not directly linked to the principal or tensor components of the strain tensor. It is however, uniquely linked to the stress tensor through the yield function and stress-strain relation, and therefore falls under the category of a stress metric.

The idea of an FLC based on the variables $(\bar{\varepsilon}_p, \alpha)$ was proposed by Yoshida et al. (2007) and the idea of an FLC based on the variables $(\bar{\varepsilon}_p, \beta)$ was proposed by Zeng et al. (2008). These ideas are illustrated in Fig. 7. The alternate diagrams are mathematically equivalent to the stress FLC for models with positive work hardening, as is evident in the one-to-one relationship between the stress

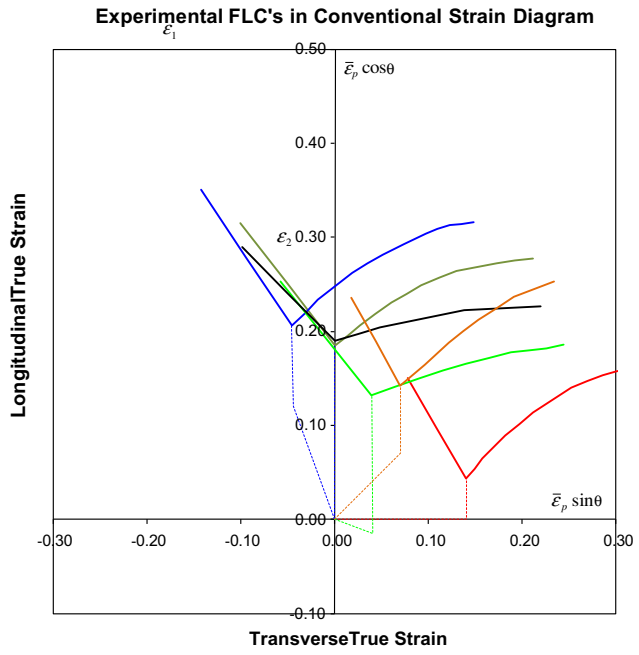


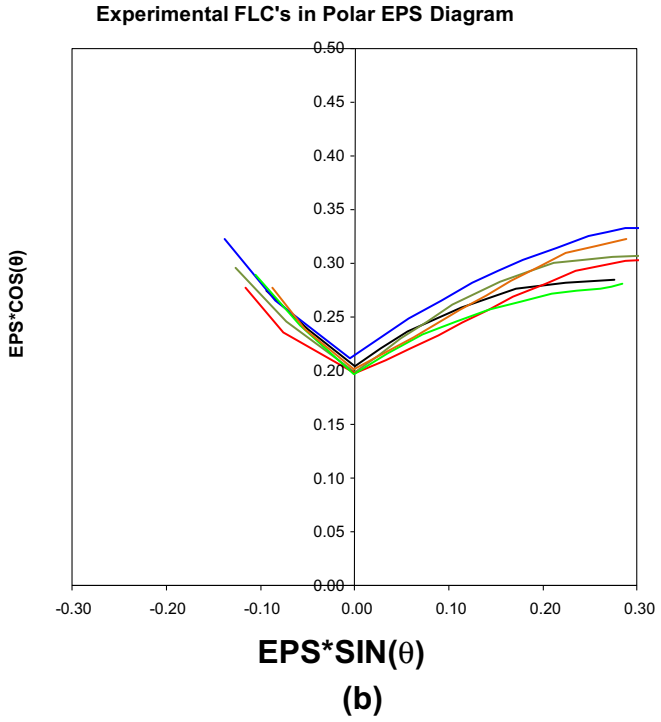


**Fig. 9.** (a) Experimental Strain FLC's of the 5 prestrain and as-received condition corresponding to the 6 Stress FLC's shown in Fig. 1. (b) Calculated EPS FLC's shown in the PEPS Diagram with the direction given by the angle defined in Eq. (12). Note that the scatter in the EPS strain is clearly on the scale of the expected experimental uncertainty.

state and the values of the alternate variables due to the monotonic hardening relationship, but these proposals have several important practical advantages: First they scale with the magnitude of strain, so it is easier to visualize safety margins for conditions that are near to the necking limit. Second, they do not depend on the stress-strain relation at all. In one sense, that means they are less complex to use; But this independence with respect to the stress-strain relation has an even bigger advantage in that the forming limit criterion might be extendable to material models in which the stress-strain relation is not monotonic.

In this paper, we propose a mathematically equivalent solution to using the $(\bar{\varepsilon}_p, \beta)$ variables as proposed by Zeng et al. (2008), which may be more appealing to industrial engineering applications. We propose to plot the data in a polar diagram of the $\bar{\varepsilon}_p$ variable with the angle defined as the arctangent of the ratio of the principal strain rates,

$$\theta = \tan^{-1}(\dot{e}_1, \dot{e}_2). \tag{12}$$

In a Cartesian equivalent system, the variables of the proposed diagram become

$$(y, x) = (\bar{\varepsilon}_p \cos(\theta), \bar{\varepsilon}_p \sin(\theta)). \tag{13}$$

We would like to emphasize to avoid confusion that there is no physical significance to the meaning of the variables (y, x) in Eq. (13). This transformation is only useful to employ standard 2D plotting software that may only accept Cartesian coordinate data. Eq. (13) is necessary to enable use of this software to plot data in what effectively becomes a polar diagram. The physically meaningful variables with respect to formability are the angle $\theta$ and the effective plastic strain, which is the radial variable in the polar diagram. The direction $\theta$ reflects the direction of the current in-plane principal plastic strain rates, in a Cartesian coordinate system superimposed on the polar diagram.

The schematic diagram to implement the Polar EPS (Polar Effective Plastic Strain) diagram is shown in Fig. 8(a) for a bilinear path. The new path is determined based on the magnitude of effective plastic strain radius and the direction of the strain increment in the conventional strain diagram used to define the direction in the new diagram by a line on the new EPS path projecting back to the origin. A general example of an arbitrary path is shown in Fig. 8 (b), where the time history of the direction of the radial expansion of the value of the EPS is determined by the local tangent of the strain history in the conventional strain diagram.

The reason the polar diagram is appealing is seen in comparison of the shape of the conventional strain-FLD and the polar diagram in Fig. 9 for the experimental FLCs reported by Graf and Hosford for linear and nonlinear strain paths. As is the case for the as-received condition in the strain-FLD, all the FLC's in the polar diagram have cusps or low points in the plane-strain condition. Furthermore, since the effective plastic strain is actually a stress metric and the radial direction in this diagram uniquely defines the stress state, it is not surprising that we see in Fig. 9(b) that the experimental FLCs for these nonlinear strain paths are insensitive to the remarkably different strain histories, just as we saw for the stress diagram in Fig. 5. Interestingly, the shape of the FLC in the polar diagram is very similar to the shape of the strain FLC for the as-received condition. Most importantly, the radial directions in the polar diagram that correspond to uniaxial, plane-strain, equal-biaxial, etc. are *parallel* to the corresponding directions in the strain FLD, which means that the application and interpretation of the polar diagram to obtain solutions to formability problems will be intuitive to engineers familiar with the strain FLD. As long as engineers understand that the diagram is different, for example, do not make the mistake of plotting net strain tensor components in the polar diagram or plot EPS values without consideration of strain path, the polar diagram could be a convenient tool for more reliable formability assessments in manufacturing. For this reason, we propose to refer to it as the PEPS FLD, to emphasize its polar nature and its radial variable defined by the effective plastic strain.

To further illustrate the practical value of this new diagram, we apply it to analysis of the unusual case reported by Ishigaki (1977)

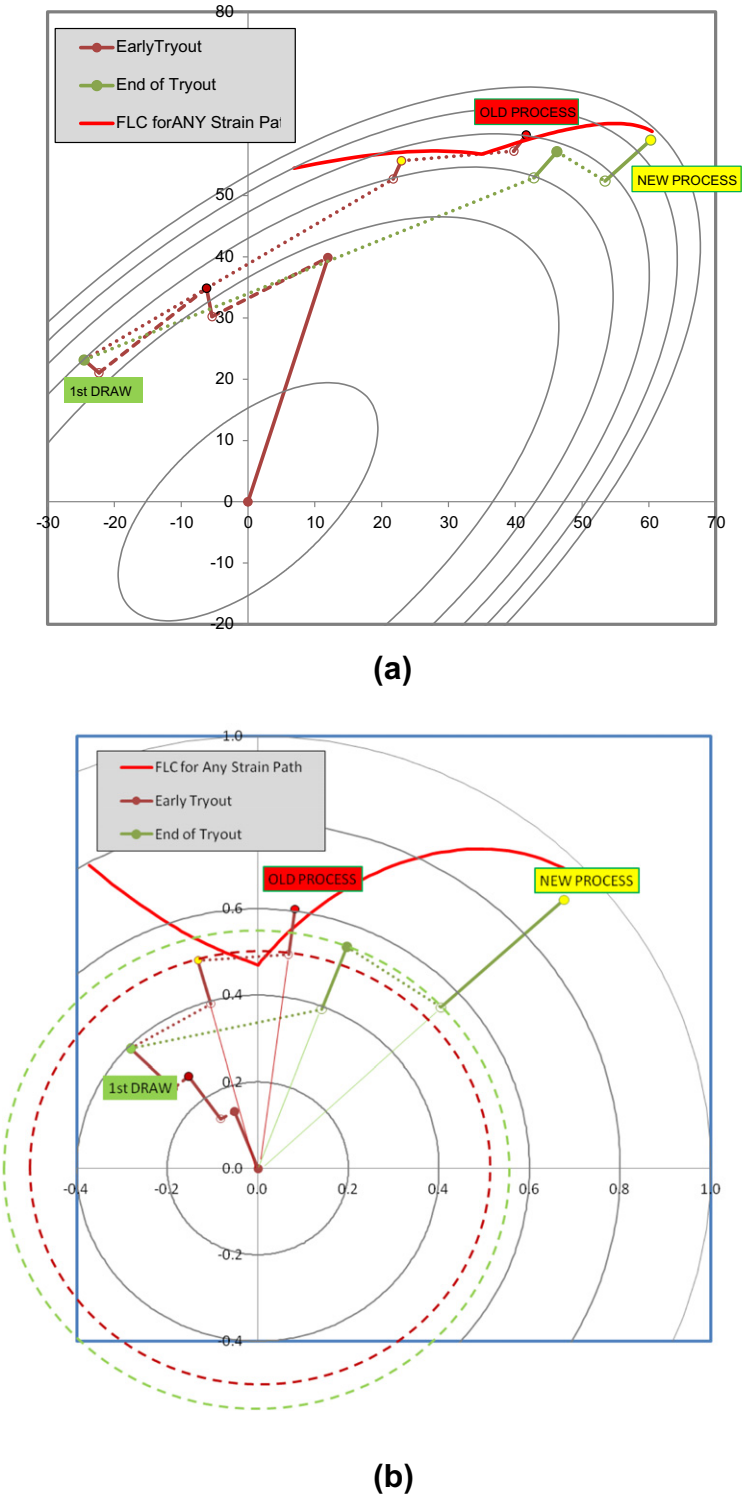


**Fig. 10.** Mapping of the experimental data in Fig. 3 into (a) stress FLD and (b) PEPS Diagram. The contours are at 20% increments in the value of EPS in both diagrams. The forming limit curve in each figure are calculated from the strain FLC for linear path, shown as the gray curve in Fig. 3. It is not necessary to experimentally determine a forming limit that applies at the end of the first draw (Stage 4), as was done to find the solution obtained by Ishigaki (1977).

described in Fig. 3. Fig. 10 shows the one-to-one mathematical correspondence of stress-based FLC and PEPS diagram for the Toyota's nonlinear concept shown in Fig. 3 by using a single path-independent forming limit curve reported for this metal. In this case both the stress diagram and the PEPS diagram provide an explanation for both the original tear observed in tryout and the robustness of the solution they obtained. This explanation is made based only on the strain-based FLC for the metal in the as-received condition, meaning that it was not necessary to measure the forming limit after Stage 4 in the stamping process, as was originally done by Ishigaki to explain the problem and solution. This is very important because the only reason the Toyota engineers were able to measure the prestrained FLC was because of two coincidences: 1)the strain at the end of the first draw form

was nearly a linear strain path and 2), the net strain at this stage happened to be very nearly a uniaxial strain condition for this metal. Had these two coincidences not occurred, the engineers would not have been able to experimentally determine how the FLC changes, and they would not have been able to explain precisely why the metal originally was tearing below the conventional strain FLC, and why they would be able to stretch the metal to such high strains. Both the stress and PEPS diagram explain both the problem and the solution. But the PEPS diagram gives the engineer a more clear picture of the margin of safety in terms of more familiar strain metrics.

Finally, the merits and limitation for PEPS diagram are summarized:

Merits :

- *There is no significant/noticeable path dependence.*
- *There is no dependence on the stress-strain relation.*
- *Shape is similar to the Strain FLC for the as-received.*

Limitation :

- *Effective strain depends on the constitutive law.*

## 5. Summary

In this paper we discussed the parameters that account for nonlinear path through the stress-based FLC and considered the same parameters in strain space. Most importantly, we proposed a new "strain-based" forming limit criterion based on a polar diagram of the effective plastic strain with the direction defined by the arctangent of the ratio of the current plastic strain rates, both of which are defined by the current stress condition, or the most recent stress condition while the material was undergoing plastic deformation. This diagram, which we refer to as the PEPS FLD in reference to its polar nature and its radial variable defined by the effective plastic strain, has advantages over the previously proposed Stress FLDs based on the principal stresses or in case of non-zero normal stress, the difference between the in-plane and through-thickness principal stresses. The primary advantages of the PEPS FLD over other diagrams based on variables with stress dimensions is the lack of dependence on the stress-strain relation and any saturation or softening that may be included in the material model. These advantages are shared by the models described by Yoshida et al. (2007) and Zeng et al. (2008) in which the limit on the effective plastic strain is characterized by the ratio of the principal stresses or ratio of the principal plastic strain rates, respectively. The primary distinction and potential appeal of the proposed PEPS FLD is that the FLC is similar in shape to the strain FLC, and the directions in the diagram corresponding to uniaxial, plane-strain, equal-biaxial, etc. are parallel to the corresponding directions in the conventional strain FLD.

## Acknowledgments

The authors would like to thank Daniel Green from University of Windsor, Xinhai Zhu from Livermore Software Technology Corporation, Ming F. Shi from United States Steel Corporation, Cedric Xia from Ford Motor Company, John Siekirk from Chrysler, Ching-Kuo Hsiung, Siguang Xu and Lumin Geng from General Motors, all for stimulating discussion and contributions to our understanding metal forming limits. The authors are particularly indebted to the reviewers of their previous papers for their thorough and critical reviews to challenge our understanding and improve our presentation of the topics covered in this and prior related papers.

## References

Arrieux, R., Bedrin, C., Boivin, M., 1982. Determination of an intrinsic forming limit stress diagram for isotropic metal sheets. In: Proceedings of the 12th Biennial Congress of the IDDRG, pp. 61–71.

Graf, A., Hosford, W.F., 1993. Effect of changing strain paths on forming limit diagrams of aluminum 2008-T 4. Metall. Trans. A24, 2503–2512.

Hill, R., 1948. A theory of the yielding and plastic flow of anisotropic metals. Proc. Roy. Soc. London A 193, 281–297.

Ishigaki, H., 1977, Deformation Analysis of Large Sized Panels in the Press Shop, Edit by D.P. Koistinen and N.M. Wang, 315-338.

Stoughton, T.B., 2000. A general forming limit criterion for sheet metal forming. Int. J. Mech. Sci. 42, 1–42.

Stoughton, T.B., Yoon, J.W., 2005. Sheet metal formability analysis for anisotropic materials under non-proportional loading. Int. J. Mech. Sci. 47, 1972–2002.

Stoughton, T.B., Yoon, J.W., 2011. A new approach for failure criterion for sheet metals. Int. J. Plasticity 27, 440–459.

Stoughton, T.B., Zhu, X., 2004. Review of theoretical models of the strain-based FLD and their relevance to the stress-based FLD. Int. J. Plasticity 20, 1463–1486.

Yoshida, K., Kuwabara, T., Kuroda, M., 2007. Path-Dependence of the Forming Limit Stresses in a Sheet Metal. Int. J. of Plasticity 23, 361–384.

Zeng, D. Chappuis, L., Xia, Z.C., and Zhu, X. 2008, A Path Independent Forming Limit Criterion for Sheet Metal Forming Simulations. SAE 2008-01-1445.